Hybrid simulations of Alfvén modes driven by energetic particles

J. Zhu*

Institute for Fusion Theory and Simulation,

Zhejiang University, Hangzhou, Zhejiang 310027, China

Z. W. Ma† and S. Wang‡

Institute for Fusion Theory and Simulation,

Zhejiang University, Hangzhou, Zhejiang 310027, China

Abstract

A hybrid kinetic-magnetohydrodynamic code (CLT-K) is developed to study nonlinear dynamics of Alfvén modes driven by energetic particles. An energetic particle mode (EPM) with a fixed frequency is first excited in the linear and early nonlinear phase. Then, a toroidal Alfvén eigenmode (TAE) comes up and gradually moves outward in the radial direction with its frequency downward chirping. In the late stage of the simulation, the TAE is suppressed due to the continuum damping and the mode becomes a energetic-particle continuum mode with the fixed frequency. The movement of the δf structure in the phase space is consistent with the mode frequency downward chirping and the drifting direction of resonance region is mainly due to the biased free energy profile. The mode structure expansion during the transition from a "central" EPM to a "edge" TAE is mainly caused by extension of the $p = 0$ trapped particle resonance in the phase space.

*Electronic address: zhu.jia@live.com

†Electronic address: zwma@zju.edu.cn

‡Electronic address: zjuws@163.com

I. INTRODUCTION

In burning plasmas, the interaction between Alfvén waves and energetic particles which come from nuclear fusion products or auxiliary heating methods is an important issue in current and future magnetic confinement fusion research[1]. Toroidicity-induced discrete shear Alfvén eigenmode (TAE)[2, 3] is one of important Alfvén waves with the frequency located inside the continuum gaps in toroidal plasmas. TAEs can be driven by energetic particles through wave-particle interaction[4, 5]. Energetic particle transport and loss associated with TAEs have attracted a lot of attention recently. On the other hand, when wave-particle interactions are strong enough to overcome continuum damping, another non-perturbative mode can be driven in the Alfvén continuum, which is called by Energetic Particle Modes[6] (EPM). One important example of an EPM is a fishbone instability[7], which can be observed usually in present tokamak experiments and its mechanism is well understood by simulations[8].

In magnetic confinement plasmas, there are two types of nonlinear scenarios for Alfvén instabilities: a slow frequency sweeping of the mode due to locking to slowly changed plasma equilibrium and a fast frequency chirping associated with a change of the fast ion distribution[9]. It is known that a discrete spectrum of toroidal Alfvén eigenmodes are determined by bulk plasma during the nonlinear stage. The nonlinear behavior of TAEs driven by energetic particles always exhibits a fast frequency chirping in current tokamak experiments[10–13]. Several nonlinear models are developed to understand TAE frequency chirping. Berk and Breizman established a model based on a bump-on-tail problem including a collision term to interpret the frequency chirping resulted from a spontaneous formation of holes and clumps in the energetic particle distribution function[14, 15]. Ge Wang et al. developed a simulation model based on the linear tip model to investigate the frequency chirping of TAEs[16]. It is found that TAEs exist with the frequency both in the gap and continuous spectrum and the TAE frequency chirps towards the upper and lower continua. Using the HAGIS code with a fixed TAE mode structure[17], Pinches et al. reproduced TAE frequency bifurcations, which agrees well with theoretical prediction and experimental observations[18]. Similar work using EAC code based on reduced model is also carried out to investigate hole-clump dynamics in phase space associated with the TAE frequency chirping[19, 20]. Many works to understand physics of the TAE frequency chirping are al-

most based on semi-analytic 1D models or reduced model with fixed mode structure, it is lack of a self-consistent simulation to capture the complex properties of the TAE frequency chirping in realistic tokamak plasmas.

It is well known that a magnetohydrodynamic (MHD) model has its limitation on imitating plasma phenomena induced by energetic particles in which kinetic effect is very important. In order to solve these problems, a hybrid model is formulated[21, 22] to include wave-particle interaction effect. A lot of numerical simulation codes based on this hybrid model have been developed to investigate energetic particle physics, such as MEGA[23, 24], HMGC[25], M3D-K[8], NIMROD[26, 27], HYM[28, 29]. Hybrid codes are powerful tools to investigate different problems of energetic particle effects on MHD activities, such as TAEs[30–36], fishbone instabilities[8], EPMs[30, 37], and tearing modes[38].

In this paper, we develop a new simulation code (CLT-K) which based on the hybrid kinetic-MHD model to study dynamical evolution of TAEs/EPMs driven by energetic particles. The framework of the MHD part is based on the CLT code[39], which is a 3D toroidal MHD code in toroidal geometries. This paper is organized as follows. In Sec. II, the simulation model and numerical method are presented. Benchmarks on a $n = 1$ TAE are shown in Sec. III. Sec. IV presents the simulation results for the $n = 2$ EPM/TAE driven by isotropic energetic ions. Finally, conclusion and discussion are given in Sec. V.

II. SIMULATION MODEL

A. A brief review of CLT

The CLT code is an initial value code that solves the full set of resistive MHD equations in toroidal geometries:

$$\frac{\partial \rho}{\partial t} = -\nabla \cdot (\rho \mathbf{v}) + \nabla \cdot [D \nabla (\rho - \rho_0)], \tag{1}$$

$$\frac{\partial p}{\partial t} = -\mathbf{v} \cdot \nabla p - \Gamma p \nabla \cdot \mathbf{v} + \nabla \cdot [\kappa \nabla (p - p_0)], \tag{2}$$

$$\frac{\partial \mathbf{v}}{\partial t} = -\mathbf{v} \cdot \nabla \mathbf{v} + [\mathbf{J} \times \mathbf{B} - \nabla p]/\rho + \nabla \cdot [\nu \nabla (\mathbf{v} - \mathbf{v}_0)], \tag{3}$$

$$\frac{\partial \mathbf{B}}{\partial t} = -\nabla \times \mathbf{E}, \tag{4}$$

$$\mathbf{E} = -\mathbf{v} \times \mathbf{B} + \eta (\mathbf{J} - \mathbf{J}_0), \tag{5}$$

$$\mathbf{J} = \frac{1}{\mu_0} \nabla \times \mathbf{B}, \tag{6}$$

where the subscript of "0" represents equilibrium variables. Equations (1)-(6) are evolved in a cylindrical coordinate system (R, ϕ, Z). A finite difference method is employed in the R and Z directions, while in the ϕ direction, either a finite difference or pseudo-spectrum method is used. In the time-advance, 4th order Runge-Kutta scheme is chosen. In the CLT code, a mixed representation (covariant for B_T and contravariant for B_P) of the axisymmetric toroidal equilibrium is used as follows:

$$\mathbf{B} = \nabla \phi \times \nabla \psi + R B_\phi \nabla \phi, \tag{7}$$

where ψ is the poloidal flux.

The benchmark on the internal kink mode and the tearing mode has been carried out to validate the credibility and applicability of CLT and the detailed descriptions can be found in Ref. [39].

B. The hybrid kinetic-MHD model

According to the current coupling formalism of the hybrid kinetic-MHD model[21, 22], only one modification in the MHD equations takes place, i.e., there is an additional contribution from energetic ion current $\mathbf{J}_h$ in the momentum equation:

$$\frac{\partial \mathbf{v}_b}{\partial t} = -\mathbf{v}_b \cdot \nabla \mathbf{v}_b + [(\mathbf{J} - \mathbf{J}_h) \times \mathbf{B} - \nabla p_b]/\rho_b + \nabla \cdot [\nu \nabla (\mathbf{v}_b - \mathbf{v}_{b0})], \tag{8}$$

where the subscript "h" and "b" are adopted to distinguish between hot particles and bulk plasma. It should be noted that $Z_h e \mathbf{E}$ does not appear in the above momentum equation

because of cancellation between $Z_h e\mathbf{E}$ and energetic particle $\mathbf{E}\times\mathbf{B}$ current. The approximation of this hybrid model is under the condition that the density of hot particle is much less than the bulk plasma density: $n_h \ll n_b$.

C. Equation of motion

We use the 5-dimensional guiding-center equations of motion derived from the Northrop guiding-center Lagrangian in the presence of the $\mathbf{E}\times\mathbf{B}$ drift velocity[40–42] to push particles in the phase space:

$$\frac{d\mathbf{X}}{dt} = \frac{1}{B_{||}^*}\left[v_{||}\mathbf{B}^* + \mathbf{E}^*\times\mathbf{b}\right], \tag{9}$$

$$\frac{dv_{||}}{dt} = \frac{Z_h e}{mB_{||}^*}\mathbf{B}^*\cdot\mathbf{E}^*, \tag{10}$$

where the modified fields $\mathbf{B}^* = \nabla\times\mathbf{A}^*$ (with $B_{\|}^* \equiv \mathbf{B}^*\cdot\mathbf{b}$ and $\mathbf{b}$ is a unit vector of the magnetic field) and $\mathbf{E}^* = -\nabla\Phi^* - \partial\mathbf{A}^*/\partial t$ are expressed in terms of the new effective electrostatic potential and the vector potential:

$$\Phi^* = \Phi + \frac{1}{Z_h e}\mu B + \frac{m}{2Z_h e}\left|\mathbf{v}_E\right|^2, \tag{11}$$

$$\mathbf{A}^* = \mathbf{A} + \frac{mv_{\|}}{Z_h e}\mathbf{b} + \frac{m}{Z_h e}\mathbf{v}_E. \tag{12}$$

It should be noted that the $\mathbf{E}\times\mathbf{B}$ drift velocity $\mathbf{v}_E = \mathbf{E}\times\mathbf{B}/B^2$ is introduced into $\mathbf{A}^*$ and the polarization drift velocity now appears explicitly in the guiding-center velocity expression (9). Here we omit the Baños drift[43] in the above equations for simplicity. The Jacobian of the guiding center transformation is $\mathscr{J}_{\rm GC} = B_{\|}^*/m$(i.e. $d\mathbf{x}d\mathbf{v} = \mathscr{J}_{\rm GC}d\mathbf{X}dv_{\|}d\mu d\alpha$), where $\mathbf{X}$ is the guiding center position,$v_{\|}$ is the parallel velocity, μ is the magnetic moment and α is the gyroangle, respectively.

D. Formalism of energetic particles current

The energetic particle current density $\mathbf{J}_h$ consists of three parts : the guiding center current $\mathbf{J}_{\rm GC}$, the magnetization current $\mathbf{J}_{\rm MAG}$, and the polarization current $\mathbf{J}_{\rm POL}$:

$$\mathbf{J}_h = \mathbf{J}_{\rm GC} + \mathbf{J}_{\rm MAG} + \mathbf{J}_{\rm POL}, \tag{13}$$

here $\mathbf{J}_{\rm GC}$ is associated with the guiding center drift velocity:

$$\mathbf{J}_{\rm GC} = \int Z_h e(\mathbf{v}_{\rm curvature} + \mathbf{v}_{\nabla B} + \mathbf{v}_B + \mathbf{v}_{EB}) f(\mathbf{X}, v_\parallel, \mu) \delta\left(\mathbf{x} - \mathbf{X} - \boldsymbol{\rho}_h\right) \mathscr{J}_{\rm GC} d\mathbf{X} dv_\parallel d\mu d\alpha, \quad (14)$$

where

$$\begin{aligned}
\mathbf{v}_{\rm curvature} &= \frac{m v_\parallel^2}{Z_h e B_\parallel^*} \nabla \times \mathbf{b}, & (15)\\
\mathbf{v}_{\nabla B} &= \frac{\mu}{Z_h e B_\parallel^*} \mathbf{b} \times \nabla B, & (16)\\
\mathbf{v}_B &= v_\parallel \frac{\mathbf{B}}{B_\parallel^*}, & (17)\\
\mathbf{v}_{EB} &= \frac{m}{Z_h e B_\parallel^*} \left[v_\parallel \nabla \times \mathbf{v}_E + \frac{1}{2} \mathbf{b} \times \nabla \left|\mathbf{v}_E\right|^2 + v_\parallel \mathbf{b} \times \frac{\partial \mathbf{b}}{\partial t} \right]. & (18)
\end{aligned}$$

The magnetization current and the polarization current can be expressed as:

$$\begin{aligned}
\mathbf{J}_{\rm MAG} &= \nabla \times \mathcal{M} = -\nabla \times \int \mu \mathbf{b} f(\mathbf{X}, v_\parallel, \mu) \delta\left(\mathbf{x} - \mathbf{X} - \boldsymbol{\rho}_h\right) \mathscr{J}_{\rm GC} d\mathbf{X} dv_\parallel d\mu d\alpha, & (19)\\
\mathbf{J}_{\rm POL} &= \int Z_h e \mathbf{v}_{\rm POL} f(\mathbf{X}, v_\parallel, \mu) \delta\left(\mathbf{x} - \mathbf{X} - \boldsymbol{\rho}_h\right) \mathscr{J}_{\rm GC} d\mathbf{X} dv_\parallel d\mu d\alpha, & (20)
\end{aligned}$$

where $\mathbf{v}_{\rm POL} = \left(m/Z_h e B_\parallel^*\right) \mathbf{b} \times \partial \mathbf{v}_E / \partial t$.

We define the guiding center density, the parallel current, the parallel and the perpendicular pressure by

$$\begin{aligned}
n_h(\mathbf{x}) &= \int f(\mathbf{X}, v_\parallel, \mu) \delta\left(\mathbf{x} - \mathbf{X} - \boldsymbol{\rho}_h\right) d\mathbf{X} dv_\parallel d\mu d\alpha,\\
N V_\parallel(\mathbf{x}) &= \int v_\parallel f(\mathbf{X}, v_\parallel, \mu) \delta\left(\mathbf{x} - \mathbf{X} - \boldsymbol{\rho}_h\right) d\mathbf{X} dv_\parallel d\mu d\alpha,\\
p_{h\parallel}(\mathbf{x}) &= \int m v_\parallel^2 f(\mathbf{X}, v_\parallel, \mu) \delta\left(\mathbf{x} - \mathbf{X} - \boldsymbol{\rho}_h\right) d\mathbf{X} dv_\parallel d\mu d\alpha,\\
p_{h\perp}(\mathbf{x}) &= \int \frac{1}{2} m v_\perp^2 f(\mathbf{X}, v_\parallel, \mu) \delta\left(\mathbf{x} - \mathbf{X} - \boldsymbol{\rho}_h\right) d\mathbf{X} dv_\parallel d\mu d\alpha,
\end{aligned}$$

respectively. Using the set of the above guiding center fluid moments, the energetic particle current density can be written as:

$$\begin{aligned}
\mathbf{J}_h &= Z_h e N V_\parallel \mathbf{b} + \frac{1}{B}\left(p_{h\parallel} - p_{h\perp}\right) \nabla \times \mathbf{b} + \frac{1}{B} \mathbf{b} \times \nabla p_{h\perp}\\
&+ \frac{m}{B} \left(N V_\parallel \nabla \times \mathbf{v}_E + \frac{n_h}{2} \mathbf{b} \times \nabla \left|\mathbf{v}_E\right|^2 + N V_\parallel \mathbf{b} \times \frac{\partial \mathbf{b}}{\partial t} \right)\\
&+ \frac{n_h m}{B} \mathbf{b} \times \frac{\partial \mathbf{v}_E}{\partial t}. \quad (21)
\end{aligned}$$

E. δf method

In order to reduce the particle noise, the δf method[44, 45] is used to calculate the energetic particle current density. We split the energetic particle current density into the equilibrium and perturbed parts: $\mathbf{J}_h = \mathbf{J}_{h0} + \delta\mathbf{J}_h$, where $\mathbf{J}_{h0}$ can be calculated by integrating an analytical distribution function. The equilibrium energetic particle distribution function can be treated as a function of three constants of motion:

$$f_0 = f_0(P_\phi, E, \Lambda), \tag{22}$$

where $P_\phi = -Z_h e\psi + mv_\parallel RB_\phi/B$ is the toroidal canonical momentum, $E = \frac{1}{2}mv_\parallel^2 + \mu B$ is the particle energy and $\Lambda = \mu B_0/E$ is the pitch-angle parameter with the magnetic field strength B_0 at the magnetic axis, μ is the magnetic moment. A new variable of the weight $w = \delta f/g$ is introduced, where g is the marker loading distribution function. The weight equation is given by

$$\frac{dw}{dt} = -\frac{1}{g}\frac{d}{dt}f_0 = -\frac{1}{g}\left[\frac{dP_\phi}{dt}\frac{\partial f_0}{\partial P_\phi} + \frac{dE}{dt}\frac{\partial f_0}{\partial E} + \frac{d\Lambda}{dt}\frac{\partial f_0}{\partial \Lambda}\right], \tag{23}$$

where

$$\frac{dP_\phi}{dt} = \left(\frac{d\mathbf{X}}{dt}\right)_1 \cdot \nabla P_\phi + \left(\frac{dv_\parallel}{dt}\right)_1 \frac{\partial P_\phi}{\partial v_\parallel}, \tag{24}$$

$$\frac{dE}{dt} = mv_\parallel \frac{dv_\parallel}{dt} + \mu\left(\frac{d\mathbf{X}}{dt}\cdot\nabla B + \frac{\partial B}{\partial t}\right), \tag{25}$$

$$\frac{d\Lambda}{dt} = -\frac{\mu B_0}{E^2}\frac{dE}{dt}. \tag{26}$$

III. BENCHMARK STUDY

Firstly, a benchmark study is carried out for a $n = 1$ TAE. A low beta tokamak equilibrium with shifted circular flux surfaces is assumed and the total volume averaged beta is $\langle\beta\rangle = 0.5\%$. The other baseline parameters for both equilibrium and energetic ions are same as in Ref. [19]. The contour plot of the radial plasma displacement $\boldsymbol{\xi}\cdot\nabla\psi$ on a poloidal cross section is shown in Fig. 1(a). We construct a flux coordinate system (ψ, θ, ϕ) which is consistent with the eigenvalue code NOVA[46] for the purpose of data analysis. Therefore, the two dimensional (2D) mode structure $\xi_\psi(R, Z)$ can be converted into the summation of the

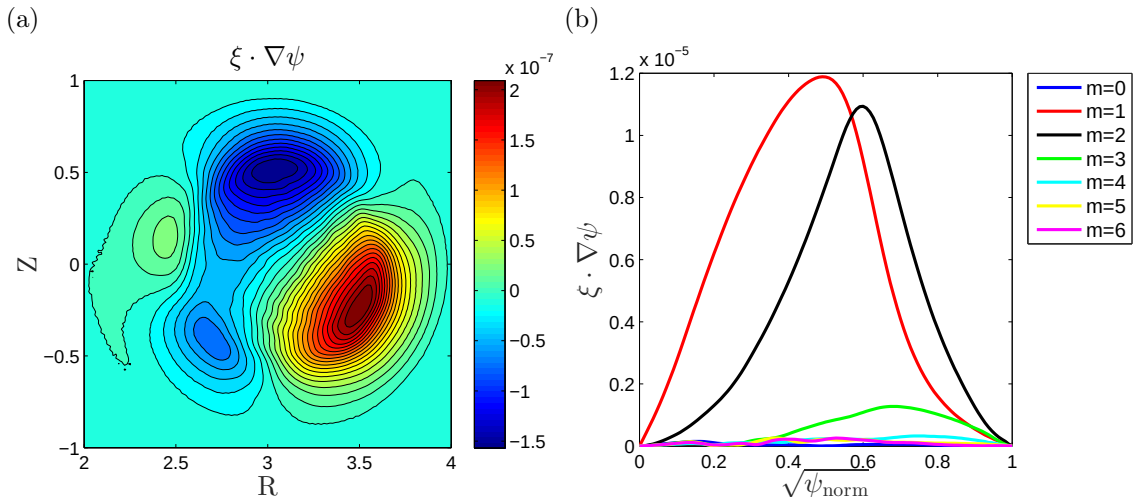

Figure 1: (a) contour plot of the mode structure $\boldsymbol{\xi} \cdot \nabla\psi$ and (b) the eigenfunction $\boldsymbol{\xi} \cdot \nabla\psi$ as the function of $\sqrt{\psi_{\rm norm}}$ for Fourier poloidal components.

absolute value of the Fourier poloidal components as a function of square root of the normalized poloidal flux $\sqrt{\psi_{\rm norm}}$. The two dominant poloidal modes are $m = 1, 2$ as shown in Fig. 1(b). It is found that both one dimensional (1D) and 2D mode structures agree well with that from the eigenvalue code NOVA[47]. We further check the frequencies of a TAE driven both by energetic particles and the external antenna. We have $\omega_{\rm EP} = 0.093\omega_A (\omega_A = v_A/a)$ and $\omega_{\rm antenna} = 0.097\omega_A$ from CLT-K, while $\omega_{\rm NOVA} = 0.1\omega_A$ from the NOVA code, i.e., the differences of all three frequencies are small. The scaling law of the linear growth rate γ_L versus the peak energetic particle beta in the CLT-K simulation is $\gamma_L/\omega\beta_{h0} = 0.578$ while NOVA predicts $\gamma_L/\omega\beta_{h0} = 1$. The large discrepancy of the linear growth rate between two codes is mainly due to the non-perturbative approach used in our code.

The benchmark study on nonlinear dynamics of the $n = 1$ TAE is also carried out. In order to reduce the linear phase, the total volume averaged beta increases to$\langle\beta\rangle = 2.0\%$ with $\beta_{\rm frac} = \langle\beta_h\rangle \,/\, \langle\beta\rangle \sim 0.75$. We can also adjust dissipation parameters (such as viscosity, diffusion, resistivity) to guarantee that the TAE mode structure remains nearly unchanged. Since the spatial scale of the $n = 1$ TAE mode as shown in Fig. 1(a) is much larger than that of the wave-particle resonance layer, there is no spatial variation for particles deeply trapped by the wave in the phase space. Thus, the main saturation mechanism in the nonlinear phase is mainly resulted from the wave-particle trapping relevant to classical bump-on-tail problem[48], which suggested that our simulation results can be comparable

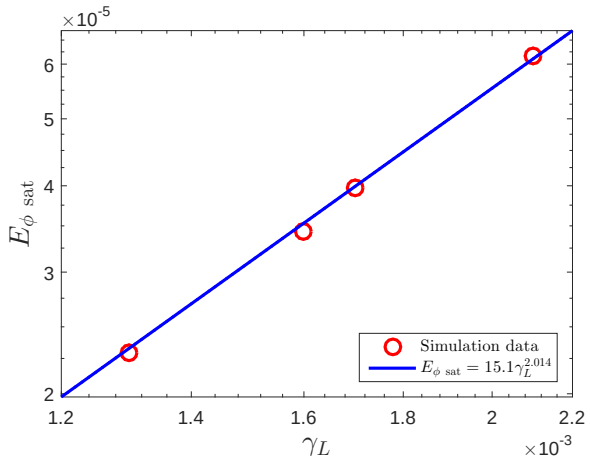

Figure 2: The nonlinear saturation level of E_ϕ versus the linear growth rate.

with Berk-Breizman theory [49] if we remove the MHD nonlinearity during the simulation. Indeed, the saturation level of the toroidal electric field in our simulation scales as $\gamma_L^{2.014}$, which is in a good agreement with the analytic prediction[49].

IV. SIMULATION RESULTS

A. n=2 modes driven by isotropic energetic ions

In this simulation, we choose the circular tokamak equilibrium with an aspect ratio of 3.0. The simulation parameters are chosen as follows: the total volume averaged beta $\langle\beta\rangle = 2\%$, the energetic ion volume averaged beta $\langle\beta_h\rangle = 1.6\%$, the particle number 5.2×10^6, and the safety factor profile $q = 1.25 + \Psi$, where Ψ is the normalized poloidal flux varying from zero at the magnetic axis to unity at the edge. The plasma density is set to be uniform. In the cylindrical coordinate (R, ϕ, Z) of CLT-K, the number of grid points is $128 \times 16 \times 128$ and the viscosity, diffusion, resistivity, and thermal conductivity are chosen to be $\nu = 5 \times 10^{-5} v_A a$, $D = 1 \times 10^{-6} v_A a$, $\eta = 1 \times 10^{-6} \mu_0 v_A a$, and $\kappa = 1 \times 10^{-6} v_A a$, respectively. The particle distribution is chosen to be a slowing down distribution in the velocity space and an exponential distribution in the real space,

$$f_0 = \frac{1}{v^3 + v_c^3}\left[1 + \mathrm{erf}\left(\frac{v_0 - v}{\Delta v}\right)\right] \exp\left(-\frac{\langle\psi\rangle}{0.37\Delta\psi}\right),$$

where $\langle\psi\rangle$ is an averaged poloidal flux over the particle orbit, which labels an effective orbit center with the given constants of motion (P_ϕ, E, μ):

$$\begin{aligned}\langle\psi\rangle &= -P_\phi/(Z_h e) + \frac{m}{Z_h e}\left\langle v_\parallel R\frac{B_\phi}{B}\right\rangle \\ &= \begin{cases} -P_\phi/(Z_h e) & , \ \mu B_0/E > 1 \text{ for trapped particles} \\ -P_\phi/(Z_h e) + \frac{m}{Z_h e}\mathrm{sgn}(v_\parallel) v R_0\sqrt{1-\mu B_0/E} & . \ \mu B_0/E \le 1 \text{ for passing particles} \end{cases}\end{aligned}$$

Fig. 3(a) shows the initial equilibrium profiles of the total pressure $p = p_b + p_h$ and the safety factor q, where p_b is the pressure of the bulk plasma and p_h is the pressure of the energetic particles. The three components of the equilibrium energetic particle current are also plotted in Fig. 3(b)-(d), which is very similar with the result of the equilibrium model including self-consistent energetic beam ion effect in Ref. [50] except for $J_{h0\phi}$, because the distribution as a monotonic function of P_ϕ is used in their results while we choose a distribution as a function of of averaged poloidal fluxes $\langle\psi\rangle$ with balanced co-going and counter-going particles.

It is found in Fig. 4 that bulk plasma kinetic energy exponentially grows in the linear phase and then reaches the saturated state at about 1600 ω_A^{-1}. The magnitude of the radial magnetic field exhibits an oscillation property in the whole simulation period as shown in Fig. 5(a). In the linear phase, its frequency remains almost unchanged around $\sim 0.1\omega_A$, while in the nonlinear stage, the mode frequency chirps down evidently and finally reaches a steady frequency about $0.05\omega_A$ as shown in Fig. 5(b). The downward chirping phenomena is very similar with that obtained from a reduced model (the EAC code)[51], although an anisotropic distribution in the pitch angle parameters Λ is adopted and the mode structure is fixed in the EAC code.

The toroidal electric field in different stages is examined. In the linear phase, the dominant poloidal mode numbers are m =2, 3 and the location of the maximum mode amplitude is around $\sqrt{\psi_{\mathrm{norm}}} \sim 0.25$. During the early nonlinear phase, the amplitude of the m =3 mode reduces and only the m =2 mode becomes dorminant. The perturbation structure of the m =2 mode shrinks and moves towards the magnetic axis. At the late stage, the $m = 3$ mode recovers and grows to be dominant and the $m = 4$ mode becomes evident. The location of the peak amplitude of the mode moves outward at $\sqrt{\psi_{\mathrm{norm}}} \sim 0.6$.

In order to examine the type of modes in our simulations, the continuum spectrum calculated by the NOVA code is shown in Fig. 7. In the linear stage, it can found that the

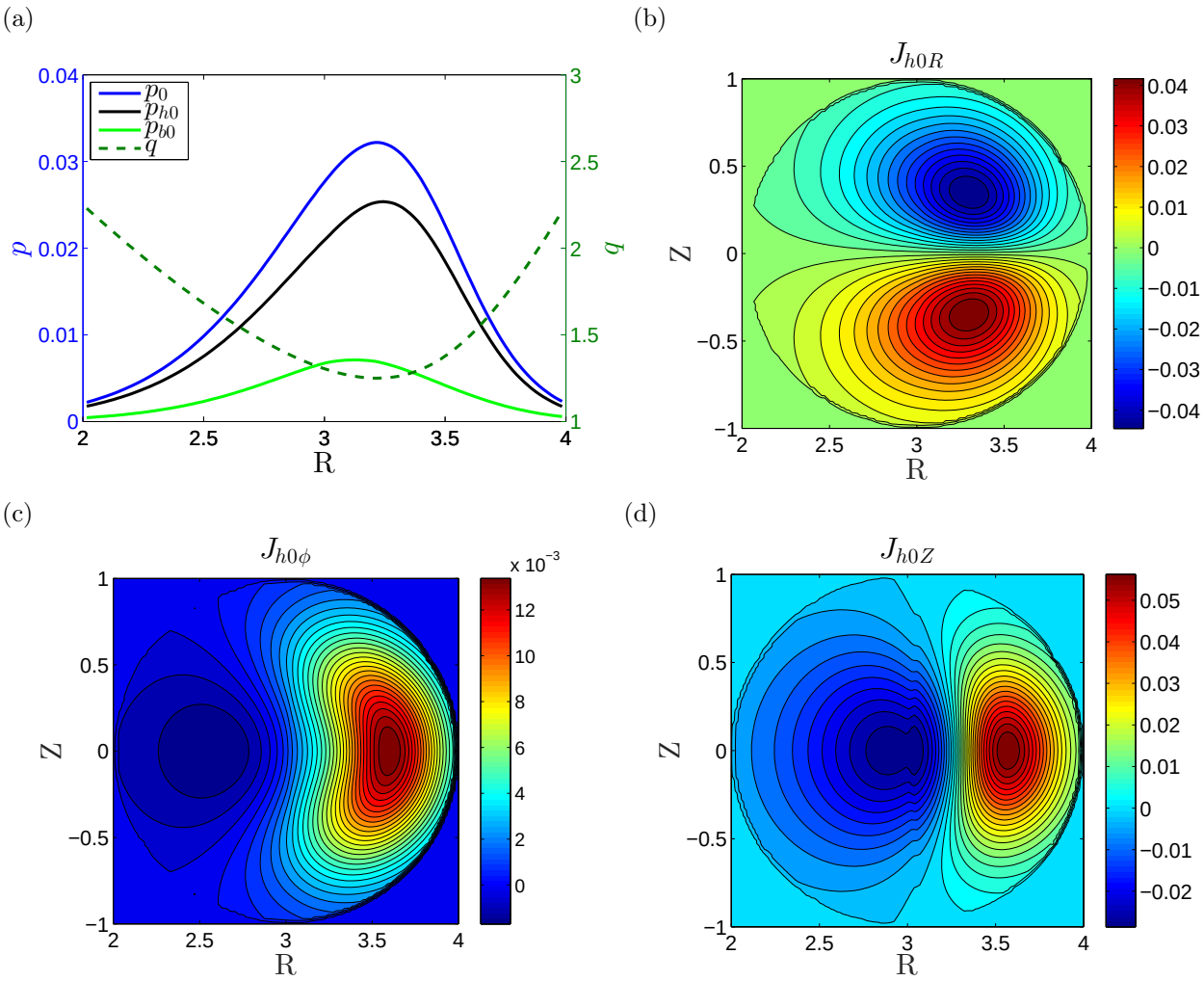

Figure 3: (a)Initial equilibrium profiles of p and q, (b) equilibrium energetic particle current J_{h0R}, (c) $J_{h0\phi}$, (d)J_{h0Z},

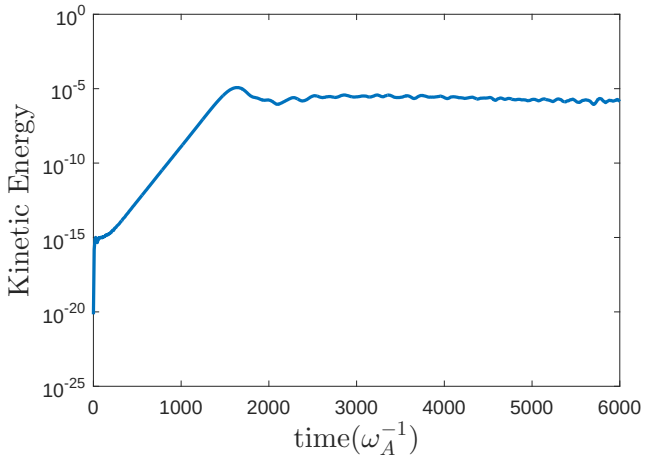

Figure 4: Time evolution of bulk plasma kinetic energy for the $n = 2$ mode

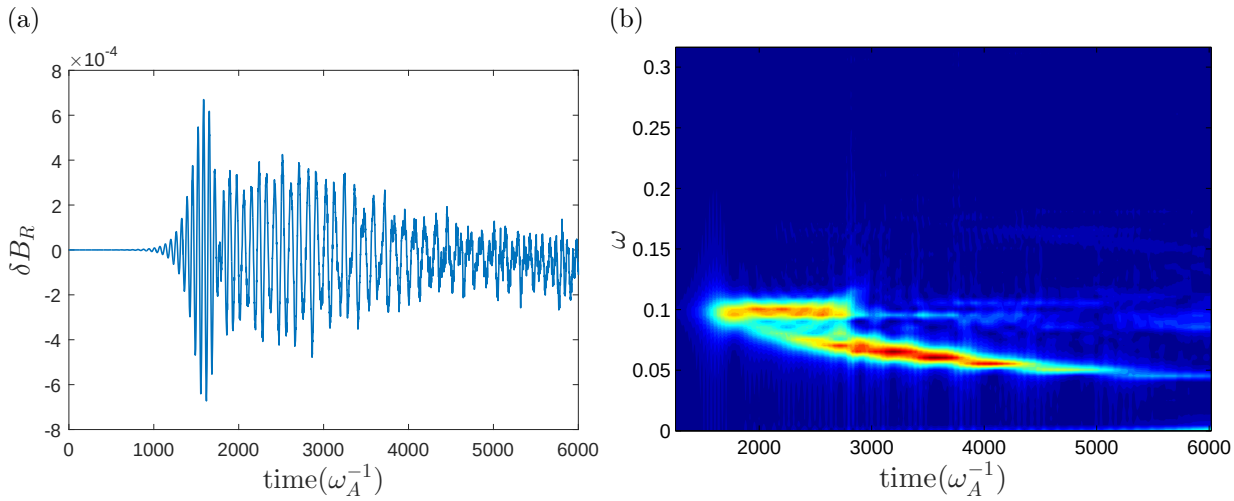

Figure 5: Time evolution of (a) the radial magnetic field near the location of the maximum mode amplitude and (b) the mode frequency

mode with its frequency $\omega = 0.1\omega_A$ is in the regime of the Alfvén continuum and the location of the maximum mode amplitude is almost at $\sqrt{\psi_{\rm norm}} \sim 0.25$, which is consistent with that in Fig. 6(a). Although the mode shows a TAE structure with double poloidal harmonics, both the mode frequency and the mode structure are determined non-perturbatively by the EP dynamics, so the linear mode (non-chirping mode) can be identified as a TAE-type EPM[52, 53] or called a resonance TAE (rTAE)[54, 55]. When the system enters into the nonlinear regime ($\sim 2000\omega_A^{-1}$), a TAE is excited near the gap location at $\sqrt{\psi_{\rm norm}} \sim 0.7$. But, when the TAE gradually moves outward in the radial direction and its frequency chirps downward, it is suppressed due to the continuum damping. The mode transit from a TAE (a gap mode) to a EPM (a non-perturbative mode) with a fixed frequency $\omega = 0.05\omega_A$.

As suggested in Ref. [51], the main physical mechanism for the downward chirping is biased driving forces associated with the negative drift of the phase island in the KAM surfaces. In the self-consistent CLT-K simulation, a tunnel induced downward chirping frequency is established due to mode conversion between the two gap mode in the gap of the alfvén continuum. In order to understand physical mechanism of the frequency downward chirping and mode structure expansion, we investigate the dynamics of the δf structure in the (E, P_ϕ) phase space. It is found in Fig. 8(a) that theδf structure of $\Lambda = 0.50$ at the linear stage shows a clear hole-clump pair structure, which is very similar with previous results both from the reduce model[19, 51] and the hybrid model[31]. Unlike non-separation

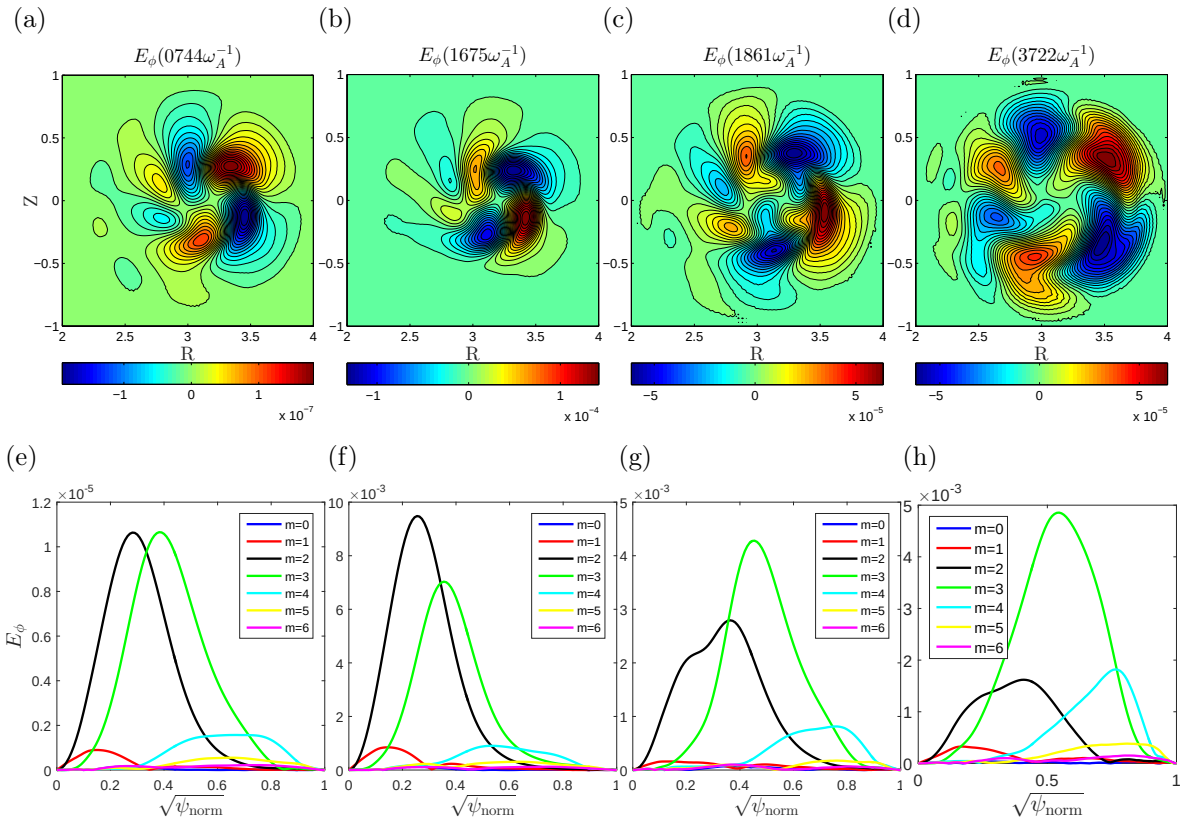

Figure 6: Toroidal component of electric field at different time

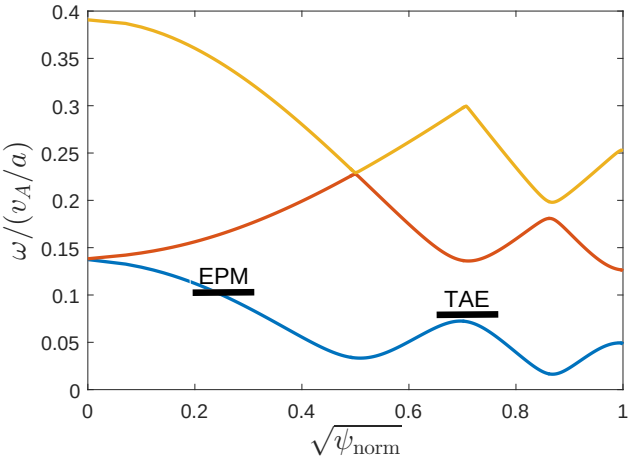

Figure 7: $n = 2$ continuum spectrum, which is obtained from the NOVA code.

of hole-clump pairs in the reduced model[51], it is interestingly to note that at the nonlinear stage the hole (blue) structure moves towards the smaller energy and larger P_ϕ region while the clump (red) structure remains in the same location. We plot resonant lines in Fig. 8 using the same particle orbit frequency analysis method[19]. The resonant line in the phase

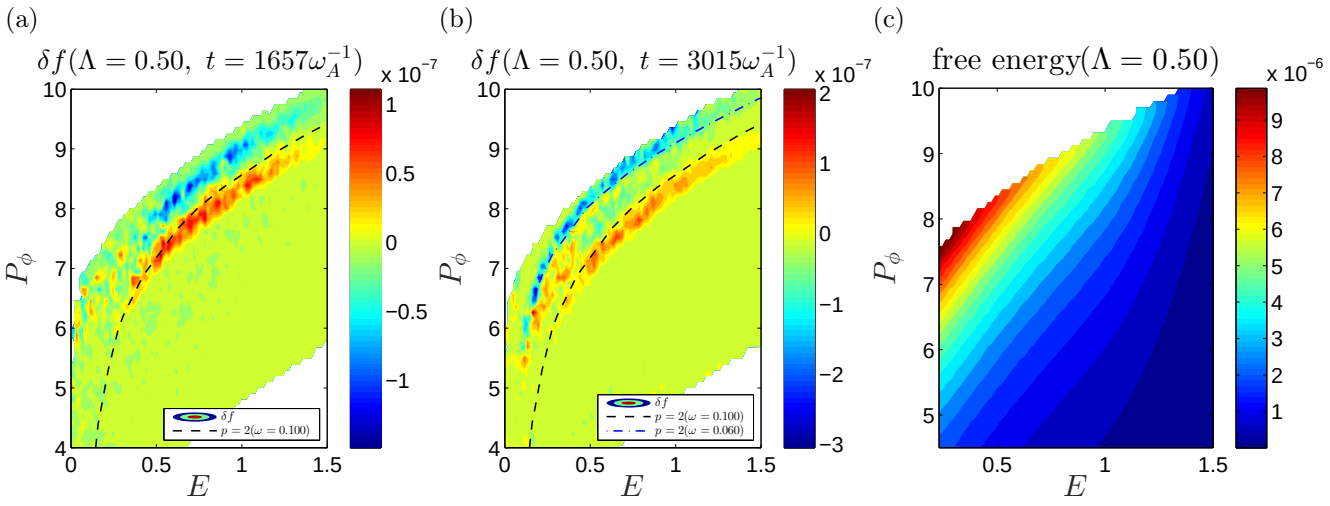

Figure 8: Comparisons of the δf structure for $\Lambda = 0.50$ at different times (a)$t = 1657\omega_A^{-1}$, (b)$t = 3015\omega_A^{-1}$ and (c) the free energy distribbution in the (E, P_ϕ) phase space.

space is determined by a constant phase $\dot{\Theta} \equiv n\omega_\phi - p\omega_\theta - \omega$, where ω_ϕ, ω_θ, n, p are the toroidal orbit frequency, the poloidal orbit frequency, the toroidal mode number, and an integer. The upward drift of the passing particle resonance line indicates that the mode frequency decreases. It is known that free energy for the isotropic energetic particles is related to the gradient of distribution functions: $\gamma(E, P_\phi, \Lambda) \propto \partial f_0/\partial E + (n/\omega)\partial f_0/\partial P_\phi$ and biased driving forces due to nonuniform distribution of the free energy can cause the asynchronous separation of hole-clump pair[51]. We check free energy profile in the (E, P_ϕ) phase space in Fig. 8(c). It is shown that the negative direction of the free energy gradient is the same with the moving direction of holes. It should be noted that the similar phenomena of resonance line motion in the phase space is also observed for the small Λcases (such as $\Lambda = 0.00, 0.25$), but it is more evident for $\Lambda = 0.50$ cases.

For the trapped particle resonance, its phase space structure is very different from the passing particle's , which is shown in Fig. 9(a) and (b). It is found that dominant $p = 0$ resonant structure is localized around the magnetic axis(large P_ϕ edge) at the early linear stage. When system enters into the nonlinear stage, the trapped particle resonance moves along the resonant line associated with the frequency downward chirping, meanwhile its radial structure extends to the smaller P_ϕ region associated with mode structure expansion outward in real space. Also, $p = -1$ resonance becomes more evident at the later nonlinear stage. Like the $\Lambda = 0.50$ cases, the movement trapped particle resonances in phase space

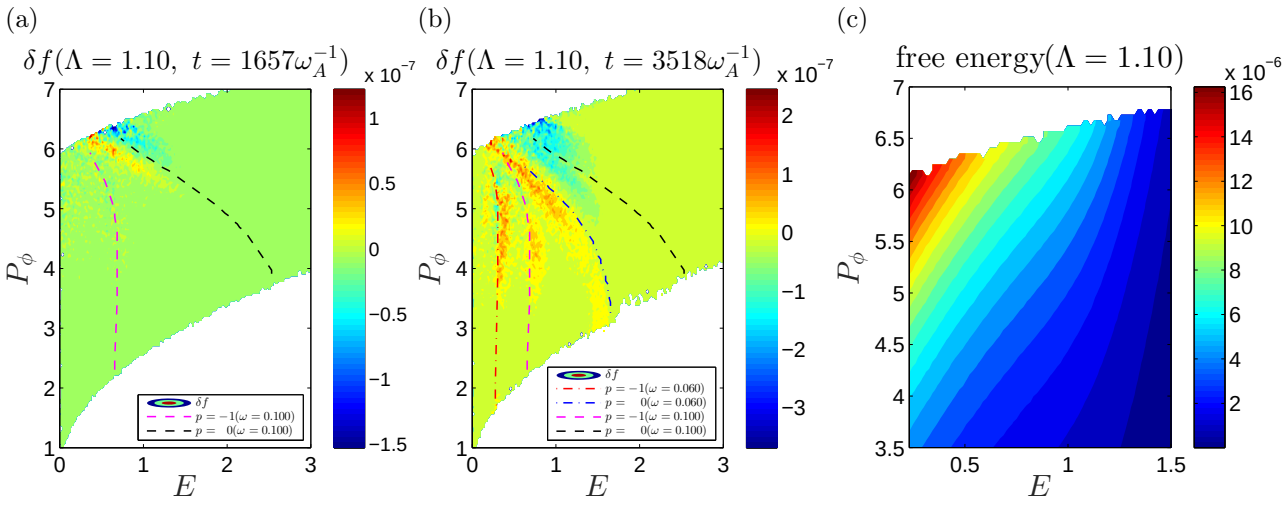

Figure 9: Comparisons of the δf structure for $\Lambda = 1.10$ at two different time (a)$t = 1657\omega_A^{-1}$ and (b)$t = 3518\omega_A^{-1}$

is also consistent with the negative direction of free energy gradient shown in Fig. 9(c). It can be concluded that the expansion of mode structure during the transition form a TAE to a EPM shown in Fig. 6 is mainly induced by nonlinear interaction between waves and trapped particles.

V. CONCLUSION

A new hybrid kinetic-MHD code (CLT-K) is developed to study the EPM/TAE driven by energetic particles, which is an extention of the original 3D toroidal MHD code (CLT) by including the effect of wave-particle interaction. Benchmark studies on a $n = 1$ TAE for both the linear and nonlinear phases have been carried out to validate our code.

For the case of a $n = 2$ single mode driven by isotropic energetic particles, frequency downward chirping and contraction-expansion process of the mode structure have been observed. At the linear and early nonlinear stage, the mode excited by energetic particles is a TAE-type EPM since its frequency is located in the Alfvén continuum and the frequency remains nearly unchanged. Then, a TAE is excited and gradually moves outward in the radial direction with its frequency downward chirping. In the late stage of the simulation, the TAE is suppressed due to the continuum damping and the mode becomes a energetic-particle continuum mode with the fixed frequency. The hole structure of passing particles resonances moves towards magnetic axis drive the frequency downward chirping while the

extension of trapped particle resonances towards small P_ϕ regions in phase space drive the mode transition from the TAE to the EPM.

Acknowledgments

We are grateful to Professor Guo-yong Fu for his useful suggestion. One of the authors (Jia Zhu) thanks Dr Wei Shen and Dr Zhichen Feng for many valuable discussions and helpful comments. This work was funded by Fundamental Research Fund for Chinese Central Universities, the ITER-CN under Grant No. 2013GB104004 and 2013GB111004, China Postdoctoral Science Foundation (Grant No. 507100-X91502), the National Natural Science Foundation of China under Grant No. 41474123 and 407103-N11601.

---

[1] N. N. Gorelenkov, S. D. Pinches, and K. Toi. Energetic particle physics in fusion research in preparation for burning plasma experiments. *Nuclear Fusion*, 54(12):125001, 2014.

[2] C. Z. Cheng, Liu Chen, and M. S. Chance. High-n ideal and resistive shear alfvén waves in tokamaks. *Annals of Physics*, 161(1):21–47, 1985.

[3] C. Z. Cheng and M. S. Chance. Low-n shear alfven spectra in axisymmetric toroidal plasmas. *Physics of Fluids*, 29(11):3695, 1986.

[4] Liu Chen. *Theory of Fusion Plasmas(Bologna: Editrice Compositori) ed J. Vaclavik, F. Troyon and E. Sindoni*, pages 327–388, 1988.

[5] G. Y. Fu and J. W. Van Dam. Excitation of the toroidicity-induced shear alfven eigenmode by fusion alpha particles in an ignited tokamak. *Physics of Fluids B: Plasma Physics*, 1(10):1949, 1989.

[6] Liu Chen. Theory of magnetohydrodynamic instabilities excited by energetic particles in tokamaks. *Physics of Plasmas*, 1(5):1519, 1994.

[7] Liu Chen, R. B. White, and M. N. Rosenbluth. Excitation of internal kink modes by trapped energetic beam ions. *Physical Review Letters*, 52(13):1122–1125, 1984.

[8] G. Y. Fu, W. Park, H. R. Strauss, J. Breslau, J. Chen, S. Jardin, and L. E. Sugiyama. Global hybrid simulations of energetic particle effects on the n=1 mode in tokamaks: Internal kink and fishbone instability. *Physics of Plasmas*, 13(5):052517, 2006.

[9] S. E. Sharapov, B. Alper, H. L. Berk, D. N. Borba, B. N. Breizman, C. D. Challis, I. G. J. Classen, E. M. Edlund, J. Eriksson, A. Fasoli, E. D. Fredrickson, G. Y. Fu, M. Garcia-Munoz, T. Gassner, K. Ghantous, V. Goloborodko, N. N. Gorelenkov, M. P. Gryaznevich, S. Hacquin, W. W. Heidbrink, C. Hellesen, V. G. Kiptily, G. J. Kramer, P. Lauber, M. K. Lilley, M. Lisak, F. Nabais, R. Nazikian, R. Nyqvist, M. Osakabe, C. Perez von Thun, S. D. Pinches, M. Podesta, M. Porkolab, K. Shinohara, K. Schoepf, Y. Todo, K. Toi, M. A. Van Zeeland, I. Voitsekhovich, R. B. White, and V. Yavorskij. Energetic particle instabilities in fusion plasmas. *Nuclear Fusion*, 53(10):104022, 2013.

[10] A. Fasoli, B. N. Breizman, D. Borba, R. F. Heeter, M. S. Pekker, and S. E. Sharapov. Nonlinear splitting of fast particle driven waves in a plasma: Observation and theory. *Physical Review Letters*, 81(25):5564–5567, 1998. PRL.

[11] M. P. Gryaznevich and S. E. Sharapov. Perturbative and non-perturbative modes in start and mast. *Nuclear Fusion*, 46(10):S942–S950, 2006.

[12] M. Podestà, R. E. Bell, N. A. Crocker, E. D. Fredrickson, N. N. Gorelenkov, W. W. Heidbrink, S. Kubota, B. P. LeBlanc, and H. Yuh. Non-linear dynamics of toroidicity-induced alfvén eigenmodes on the national spherical torus experiment. *Nuclear Fusion*, 51(6):063035, 2011.

[13] M. Podestà, R. E. Bell, A. Bortolon, N. A. Crocker, D. S. Darrow, A. Diallo, E. D. Fredrickson, G. Y. Fu, N. N. Gorelenkov, W. W. Heidbrink, G. J. Kramer, S. Kubota, B. P. LeBlanc, S. S. Medley, and H. Yuh. Study of chirping toroidicity-induced alfvén eigenmodes in the national spherical torus experiment. *Nuclear Fusion*, 52(9):094001, 2012.

[14] H. L. Berk, B. N. Breizman, and N. V. Petviashvili. Spontaneous hole-clump pair creation in weakly unstable plasmas. *Physics Letters A*, 234(3):213–218, 1997.

[15] H. L. Berk, B. N. Breizman, and N. V. Petviashvili. Erratum. *Physics Letters A*, 238(6):408, 1998.

[16] Ge Wang and H. L. Berk. Simulation and theory of spontaneous tae frequency sweeping. *Nuclear Fusion*, 52(9):094003, 2012.

[17] S. D. Pinches, L. C. Appel, J. Candy, S. E. Sharapov, H. L. Berk, D. Borba, B. N. Breizman, T. C. Hender, K. I. Hopcraft, G. T. A. Huysmans, and W. Kerner. The hagis self-consistent nonlinear wave-particle interaction model. *Computer Physics Communications*, 111(13):133–149, 1998.

[18] S. D. Pinches, H. L. Berk, M. P. Gryaznevich, S. E. Sharapov, and Jet-Efda Contributors.

Spectroscopic determination of the internal amplitude of frequency sweeping tae. *Plasma Physics and Controlled Fusion*, 46(7):S47–S57, 2004.

[19] J. Zhu, G. Y. Fu, and Z. W. Ma. Nonlinear dynamics of toroidal alfveťn eigenmodes driven by energetic particles. *Physics of Plasmas*, 20(7):072508, 2013.

[20] J. Zhu, Z. W. Ma, and G. Y. Fu. Dynamic evolutions of multiple toroidal alfvén eigenmodes with energetic particles. *Physics of Plasmas*, 20(12):122508, 2013.

[21] W. Park, S. Parker, H. Biglari, M. Chance, L. Chen, C. Z. Cheng, T. S. Hahm, W. W. Lee, R. Kulsrud, D. Monticello, L. Sugiyama, and R. White. Three-dimensional hybrid gyrokinetic-magnetohydrodynamics simulation. *Physics of Fluids B: Plasma Physics*, 4(7):2033, 1992.

[22] W. Park, E. V. Belova, G. Y. Fu, X. Z. Tang, H. R. Strauss, and L. E. Sugiyama. Plasma simulation studies using multilevel physics models. *Physics of Plasmas*, 6(5):1796, 1999.

[23] Y. Todo, T. Sato, K. Watanabe, T. H. Watanabe, and R. Horiuchi. Magnetohydrodynamic vlasov simulation of the toroidal alfven eigenmode. *Physics of Plasmas*, 2(7):2711, 1995.

[24] Y. Todo and T. Sato. Linear and nonlinear particle-magnetohydrodynamic simulations of the toroidal alfven eigenmode. *Physics of Plasmas*, 5(5):1321, 1998.

[25] S. Briguglio, G. Vlad, F. Zonca, and C. Kar. Hybrid magnetohydrodynamic-gyrokinetic simulation of toroidal alfven modes. *Physics of Plasmas*, 2(10):3711, 1995.

[26] Charlson C. Kim, Carl R. Sovinec, and Scott E. Parker. Hybrid kinetic-mhd simulations in general geometry. *Computer Physics Communications*, 164(1-3):448–455, 2004.

[27] Charlson C. Kim and Nimrod team the. Impact of velocity space distribution on hybrid kinetic-magnetohydrodynamic simulation of the (1,1) mode. *Physics of Plasmas*, 15(7):072507, 2008.

[28] E. V. Belova, S. C. Jardin, H. Ji, M. Yamada, and R. Kulsrud. Numerical study of tilt stability of prolate field-reversed configurations. *Physics of Plasmas*, 7(12):4996, 2000.

[29] Elena V. Belova, Ronald C. Davidson, Hantao Ji, and Masaaki Yamada. Kinetic effects on the stability properties of field-reversed configurations. ii. nonlinear evolution. *Physics of Plasmas*, 11(5):2523, 2004.

[30] S. Briguglio, F. Zonca, and G. Vlad. Hybrid magnetohydrodynamic-particle simulation of linear and nonlinear evolution of alfven modes in tokamaks. *Physics of Plasmas*, 5(9):3287, 1998.

[31] Jianying Lang, Guo-Yong Fu, and Yang Chen. Nonlinear simulation of toroidal alfven eigenmode with source and sink. *Physics of Plasmas*, 17(4):042309, 2010.

[32] Y. Todo, H. L. Berk, and B. N. Breizman. Nonlinear magnetohydrodynamic effects on alfvén eigenmode evolution and zonal flow generation. *Nuclear Fusion*, 50(8):084016, 2010.

[33] Y. Todo, H. L. Berk, and B. N. Breizman. Simulation of alfvén eigenmode bursts using a hybrid code for nonlinear magnetohydrodynamics and energetic particles. *Nuclear Fusion*, 52(3):033003, 2012.

[34] Y. Todo. Nonlinear simulations of alfven eigenmodes destabilized by energetic particles. *AIP Conference Proceedings*, pages 141–154, 2012.

[35] Y. Todo, M. A. Van Zeeland, A. Bierwage, and W. W. Heidbrink. Multi-phase simulation of fast ion profile flattening due to alfvén eigenmodes in a diii-d experiment. *Nuclear Fusion*, 54(10):104012, 2014.

[36] Y. Todo, M. A. Van Zeeland, A. Bierwage, W. W. Heidbrink, and M. E. Austin. Validation of comprehensive magnetohydrodynamic hybrid simulations for alfvén eigenmode induced energetic particle transport in diii-d plasmas. *Nuclear Fusion*, 55(7):073020, 2015.

[37] Y. Todo. Properties of energetic-particle continuum modes destabilized by energetic ions with beam-like velocity distributions. *Physics of Plasmas*, 13(8):082503, 2006.

[38] Huishan Cai and Guoyong Fu. Hybrid simulation of energetic particle effects on tearing modes in tokamak plasmas. *Physics of Plasmas*, 19(7):072506, 2012.

[39] S. Wang and Z. W. Ma. Influence of toroidal rotation on resistive tearing modes in tokamaks. *Physics of Plasmas*, 22(12):122504, 2015.

[40] John R. Cary and Alain J. Brizard. Hamiltonian theory of guiding-center motion. *Reviews of Modern Physics*, 81(2):693–738, 2009.

[41] T. S. Hahm. Nonlinear gyrokinetic equations for turbulence in core transport barriers. *Physics of Plasmas*, 3(12):4658, 1996.

[42] H. Qin, R. H. Cohen, W. M. Nevins, and X. Q. Xu. General gyrokinetic equations for edge plasmas. *Contributions to Plasma Physics*, 46(7-9):477–489, 2006.

[43] Baños. The guiding centre approximation in lowest order. *Journal of Plasma Physics*, 1(3):305–316, 1967.

[44] S. E. Parker and W. W. Lee. A fully nonlinear characteristic method for gyrokinetic simulation. *Physics of Fluids B: Plasma Physics*, 5(1):77–86, 1993.

[45] Genze Hu and John A. Krommes. Generalized weighting scheme for f particle-simulation method. *Physics of Plasmas*, 1(4):863, 1994.

[46] C. Z. Cheng and M. Chance. Nova: A nonvariational code for solving the mhd stability of axisymmetric toroidal plasmas. *Journal of Computational Physics*, 71(1):124–146, 1987.

[47] N. N. Gorelenkov. Varification and validation (vv) of energetic particle (ep) driven instabilities, 2008.

[48] Ira Bernstein, John Greene, and Martin Kruskal. Exact nonlinear plasma oscillations. *Physical Review*, 108(3):546–550, 1957.

[49] H. L. Berk and B. N. Breizman. Saturation of a single mode driven by an energetic injected beam. iii. alfven wave problem. *Physics of Fluids B: Plasma Physics*, 2(9):2246, 1990.

[50] E. V. Belova, N. N. Gorelenkov, and C. Z. Cheng. Self-consistent equilibrium model of low aspect-ratio toroidal plasma with energetic beam ions. *Physics of Plasmas*, 10(8):3240, 2003.

[51] J. Zhu, Z. W. Ma, and G. Y. Fu. Nonlinear frequency chirping of toroidal alfvén eigenmodes in tokamak plasmas. *Nuclear Fusion*, 54(12):123020, 2014.

[52] Fulvio Zonca and Liu Chen. Destabilization of energetic particle modes by localized particle sources. *Physics of Plasmas*, 7(11):4600, 2000.

[53] Alexey Mishchenko, Axel Konies, and Roman Hatzky. Global particle-in-cell simulations of fast-particle effects on shear alfven waves. *Physics of Plasmas*, 16(8):082105, 2009.

[54] C. Z. Cheng, N. Gorelenkov, and C. T. Hsu. Fast particle destabilization of toroidal alfven eigenmodes. *Nuclear Fusion*, 35(12):1639–1650, 1995.

[55] N. Gorelenkov, S. Bernabei, C. Z. Cheng, K. W. Hill, R. Nazikian, S. Kaye, Y. Kusama, G. Kramer, K. Shinohara, Ozeki. T., and M. Gorelenkova. Stability properties of toroidal alfvén modes driven by fast particles. *Nuclear Fusion*, 40(7):1311–1323, 2001.